Quantitative evaluation of the mechanical strength of titanium/composite bonding using laser-generated shock waves

Mathieu Ducousso, Simon Bardy, Yann Rouchausse, Tomas Bergara, Frédéric Jenson, Laurent Berthe, Nicolas Cuvillier

Quantitative evaluation of the mechanical strength of titanium/composite bonding using laser-generated shock waves

M. Ducousso,[1,a)] S. Bardy,[2] Y. Rouchausse,[3] T. Bergara,[4] F. Jenson,[1] L. Berthe,[3] L. Videau,[2] and N. Cuvillier[1]
[1]*Safran Tech, Rue des jeunes Bois, 78114 Magny les Hameaux, France*
[2]*CEA, DAM, DIF, F-91297 Arpajon, France*
[3]*Laboratoire Procédés et Ingénieries en Mécanique et Matériaux, CNRS, Arts et Métiers Paris Tech, 151 Bd de l'Hôpital, 75013 Paris, France*
[4]*Rescoll, 8 Allée Geoffroy Saint-Hilaire, 33600 Pessac, France*

Intense acoustic shock waves were applied to evaluate the mechanical strength of structural epoxy bonds between a TA6V4 titanium alloy and a 3D woven carbon/epoxy composite material. Two bond types with different mechanical strengths were obtained from two different adhesive reticulations, at 50% and 90% of conversion, resulting in longitudinal static strengths of 10 and 39 MPa and transverse strengths of 15 and 35 MPa, respectively. The GPa shock waves were generated using ns-scale intense laser pulses and reaction principles to a confined plasma expansion. Simulations taking into account the laser–matter interaction, plasma relaxation, and non-linear shock wave propagation were conducted to aid interpretation of the experiments. Good correlations were obtained between the experiments and the simulation and between different measurement methods of the mechanical strength (normalized tests vs laser-generated shock waves). Such results open the door toward certification of structural bonding. https://doi.org/10.1063/1.5020352

In 2012, the aviation industry adopted an ambitious set of commitments (for instance, to stop the growth of CO_2 emissions by 2020 and to halve emissions by 2050 compared to 2005 levels) to reduce its contribution to global climate changes.[1] One approach is to use lighter structural materials, such as composite materials. However, one main limitation of their use concerns their assembly. Namely, they cannot be welded nor attached using rivets. Thus, bonding is often the only way to attach one composite structure to another. Moreover, bonding can be seen as a "smart" attachment process, as it is compatible with almost all materials, it reduces the weight of the attachment, and it is available from the conception of a structure to its repair.

The main limitation of structural bonding in the aircraft industry concerns the ability to certify in a non-invasive way the good quality of the bonding, i.e., to certify that it can resist up to a predefined strength value.[2] To date, however, no method for such certification has yet been demonstrated. Thus, there is a need to identify a quantitative non-destructive evaluation (NDE), able to certify the good quality of structural bonding, to allow further generalization of the use of composites in the transportation industry. This in turn will contribute to the expected CO_2 emission reduction.

Several NDE approaches have been investigated to realize such certification. However, as bonding quality depends on a variety of factors, including chemical (surface treatment, surface pollution…), physical (thickness, reticulation, anchorage…), and morphological (porosities and ageing), such evaluation is challenging.[3] Thermal, tomographic, electromagnetic, and optical methods have already been investigated, but presently none of them allow quantification of the mechanical strength of bonding. Intuitively, acoustic approaches appear to be more adapted to such quantification, as ultrasound is a technique based on mechanical displacement. Acoustic methods can be based on investigating the reflection or transmission of bulk waves at bonding interfaces,[4,5] using thickness resonances or guided waves.[6,7] Nonlinear approaches can also be used.[8] Nevertheless, all these approaches are applied under academic bonds of low mechanical strength and none of them enables an absolute mechanical quantification of the tested bond.[5,7] Therefore, despite the interest in such results, structural bonding certification is still far from being realized.

We propose here to use the laser-generated shock wave—or the laser adhesion test (LASAT)[9]—to evaluate the real industrial structural bonding of a titanium alloy (TA6V4) plate adhered to a composite material using a structural epoxy glue of high fracture toughness and peel strength. LASAT has been described in detail.[9] It consists of generating a plasma by the laser illumination of a sample, in the GW/cm^2 intensity range. Using ns-scale laser pulses, it is found that the temporal duration of the plasma expansion is similar to the laser pulse duration. Such plasma expansion induces an intense stress, which propagates into the material. The temporal profile and duration of the wave are similar to those of the plasma expansion at the surface. The amplitude of the stress depends mainly on the laser pulse energy and on the material at the surface of the target.[10] Into a finite thickness target, the shock wave is reflected from the back face of the material. Boundary conditions (amplitude free) induce a phase change at the reflection, and the compressive shock wave becomes a release shock wave. This release wave is

used to test the quality—or the mechanical strength—of a bond. NDE, for example, ultrasonic inspection, must be performed after the experiments to detect any bonding failure that may have occurred. LASAT has already been successfully used to investigate composite bonding in unidirectional carbon fiber-reinforced polymers (CRFPs), but its application was limited to very thin bonds of low mechanical strength, with the main limitation being that LASAT created a delamination into the bulk of the composite before the adhesion test.[11,12]

In this work, the composite material used is a thick 3D woven carbon/epoxy composite (3D-CFRP) obtained from resin transfer molding. This material contains carbon fibers that are woven together in an interlocked 3D matrix, and as a consequence, its tolerance capability upon impact is significantly increased compared to bidirectional CFRP.[13] This paper is organized as follows: First, the high tolerance of this composite material with respect to the process will be demonstrated. Second, we will present simulations of LASAT experiments on TA6V4 bonded onto a 3D-CFRP. We will demonstrate that, depending on the illuminated face of the bonding, different acoustic phenomena due to the acoustic impedance break into the structure are involved. Finally, after explaining the experimental procedure, the results will be presented and discussed.

All the experiments presented in this paper were performed on the Hephaistos laser facility at the PIMM laboratory (Laboratoire Procédés et Ingénieries en Mécanique et Matériaux). This is a 532 nm frequency-doubled Nd:YAG table-top facility of 7 ns pulse duration at full width at half maximum (FWHM). It delivers up to 14 J per pulse at a 2 Hz repetition rate. The laser spot diameter is 6 mm at the surface of the sample. We also used a water confinement regime at the surface of the materials to increase the induced stress amplitude by a factor from 5 to 10 compared to direct conditions.[10]

The non-destructive effect of the laser shock wave experiments on the composite material was demonstrated by subjecting different samples to 1, 3, and 5 successive laser shots, at the same points, at the maximum available laser fluence. Thus, these experiments of maximal laser fluence and several numbers of laser shots at the same point were strongly more soliciting for the materials than the LASAT which requires a single laser shot of less laser fluence. An aluminum adhesive of about 100 μm in thickness was placed at the surface of the samples to prevent plasma-induced thermal damage. After the experiments, the samples were inspected using ultrasonic (transmission configuration into water immersion, 15 MHz) and micro-tomographic (voxel size of 8 μm) NDEs. These NDEs did not indicate any damage to the samples that were illuminated just once. For the samples exposed to multiple laser shots, very small failures near the back surface were detected by both NDEs. Then, the samples' mechanical properties were evaluated using a normalized procedure for damage impact.[14] For all the impacted samples, the mechanical properties were identical to the non-illuminated reference samples. As this damage test was performed under much harsher conditions compared to the single-shot LASAT, it was then assumed that the LASAT process was non-invasive for the 3D-CFRP material.

Simulations of the LASAT applied to the TA6V4/3D-CFRP bonding were performed using the ESTHER code to quantify the experiments and to aid our understanding of the induced phenomena. ESTHER is a mono-dimensional Lagrangian code that describes both laser–matter interaction and shock propagation in materials.[15] The laser energy deposition is calculated by solving the Helmholtz equation.[16,17] ESTHER describes the material evolution from the solid to the plasma state by taking into account various physical phenomena such as optical absorption, reflection and transmission, heat conduction, ionization, and radiative transfer. Thus, it allows simulation of the induced pressure field in the target. Shock wave propagation into the multilayer is then simulated by the resolution of the {mass, momentum, motion quantity, and energy} equations with an adapted equation of states to rely energy and stress.[18] We used the Steinberg-Cochran-Guinan formalism for the TA64V[19] and the Mie-Grüneisen formalism for the epoxy glue and the composite modeling.[20] Illustrations of the simulations are presented in Fig. 1. The setup assumed a homogenized composite material bonded to a TA6V4 plate with an epoxy glue. The respective thicknesses were 3.8 mm, 0.4 mm, and 0.15 mm. Simulations were performed for an illumination of the TA6V4 [Figs. 1(a) and 1(c)] and the composite [Figs. 1(b) and 1(d)] with a laser intensity of 3 GW/cm^2. For both simulations, the plasma pressure was 4 GPa and its duration was 15 ns at FWHM in agreement with previous confined interaction characterization.[10] Time–position (X-t) diagrams of the shock wave propagation are reported in Figs. 1(a) and 1(b), and the induced stress at the composite/epoxy (dotted red line) and epoxy/TA6V4 (continuous blue line) interfaces for both illumination configurations is presented in Figs. 1(c) and 1(d).

First, the shock wave generation and first acoustic path into the bulk of the structure are considered. At the time of generation, the pressure spatial profile is a steep wavefront followed by an exponentially shaped decrease. This shock wave profile, beginning immediately after generation, is remarkable as, in general, shock waves in solids appear after a minimal critical distance of propagation.[21] For bonding evaluation, structures as thin as the wavelength can thus be inspected as there is no minimal distance to create a shock wave. After some propagation, the spatial pulse profile of the shock wave expands because the ridge of the wave propagates more quickly than its hollow. This has been simulated using ESTHER. In TA6V4, the acoustic wavelength is close to 100 μm after 0.4 mm of propagation and to 130 μm after 1.6 mm of propagation (i.e., 4 acoustic travels into the TA6V4 layer). In the composite material, the acoustic wavelength is close to 220 μm after 0.4 mm of propagation and to 400 μm after 3.6 mm (i.e., the thickness of the 3D-CFRP).

From the (X-t) diagrams, Figs. 1(a) and 1(b), we observed a variation of the wave propagation into the assembly as a function of the illuminated material. When illuminating the TA6V4, the acoustic wavelength is smaller than the TA6V4 thickness. Thus, multiple reflections onto its interfaces appear, creating a periodic signal of $f = v_{Ti}/2h_{Ti} \approx 80$ MHz, where v_{Ti} and h_{Ti} are the TA6V4 acoustic velocity and thickness, respectively. Such a signal is all the more observable as the refection coefficient at the

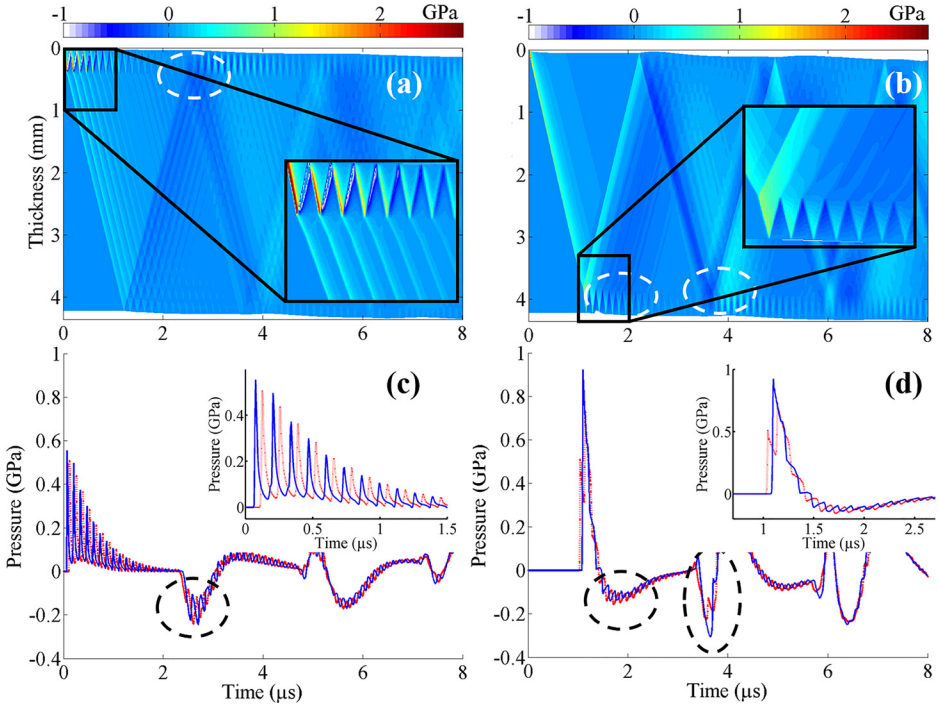

FIG. 1. Time–position (X-t) stress diagram (a) and (b) of the shock wave propagation into TA6V4/composite bonding as a function of the illuminated material: TA6V4 on the left and composite on the right. Stress (c) and (d) at the composite/epoxy (red dotted line) and epoxy/TA6V4 (blue continuous line) interfaces for both illumination configurations are also presented. For each plot, a zoom is also presented into a 1 μs/1 mm spatio-temporal window for plots (a) and (b) and 1.5 μs for plots (c) and (d). The two tiny irregular white bands along the horizontal edges of (a) and (b) are related to the 1D nature of the ESTHER Lagrangian code, which cannot model boundary conditions at lateral borders and, thus, cannot model a recall force.

TA6V4/epoxy interface is around 0.8 and the largest part of the shock wave is confined into the TA6V4 layer. However, at each reflection, part of the shock wave is transmitted into the epoxy layer and into the composite. The pressures at the epoxy interfaces are presented in Fig. 1(c) (zoom). As the acoustic wavelength ($\sim$100 μm) is smaller than the epoxy thickness, the spatial profile is similar at both interfaces and we only observed a time translation-like shape. Then, shock waves propagate into the bulk of the composite, are reflected at the back face of the structure with a phase shift, and travel back toward the epoxy layer as a release wave. The LASAT tensile stress in the glue layer appears at a time of around 2.7 μs [Fig. 1(c)], after traveling a distance of 7.8 mm into the composites.

The stress plots at the epoxy interfaces when illuminating the composite show quite a different situation [zoom into Fig. 1(d)]. Indeed, they are significantly different at both interfaces. This is related to the acoustic wavelength of the shock wave (400 μm after 3.8 mm of acoustic propagation), around three times larger than the epoxy layer thickness. Thus, the associated phenomenon in the epoxy layer is a resonance, and the time translation-like shape is no longer valid. After a transmission at the two interfaces of the glue layer, the shock is reflected at the back face of the TA6V4 layer with a phase shift and travels back toward the epoxy layer as a release wave, at a time of around 1.5 μs [Fig. 1(d)].

One can also identify the time when the maximum tensile stress occurs, and the history of the corresponding shock wave, from the (X-t) diagrams and pressure plots at the epoxy interfaces. The bonding can only be evaluated if the pressure at the epoxy interfaces is in the tensile region (dotted circled areas). As previously mentioned, the LASAT traction appears at around 2.7 μs into the TA6V4 illumination procedure, with a negative pressure of around -0.25 GPa. When illuminating the composite material, tensile stresses appear twice at the bond interface, at around 1.7 μs and 3.6 μs. The main differences between the acoustic paths related to these stresses are that for the first stress, the path is equal to one time the composite thickness and two transmissions occur at the epoxy/TA6V4 interface, while for the second stress, the path is three times the composite thickness and one reflection occurs at the epoxy/TA6V4 interface. The phase changes are related to reflection at the back and front face, respectively. These differences impact both the time duration and the value of the stresses, as the first one takes around 1.8 μs and is simulated at -0.15 GPa, while the second takes around 350 ns and is at -0.30 GPa. This simple description highlights the influence of the impedance breaks on the assembly for the LASAT process. In our configuration, this collapse exerts a larger influence than attenuation on the composite materials and creates an unprecedented LASAT configuration where phase shift reflection necessary to the LASAT process occurred at the surface of the sample. Moreover, for the same laser parameters, the ESTHER simulations predict a tensile strain at the epoxy interface $\sim$20% larger when illuminating the composite than when illuminating the TA6V4.

Four TA6V4/composite bonds with two different mechanical strengths were realized. The lateral dimensions were 240×40 mm^2. The bonding was performed using an aeronautic industrial epoxy glue from 3M industry named AF191K. For each bonded assembly, a material of around 5 mm large is used on the border, between the composites and the TA6V4 to control the thickness of the glue layer and to prevent glue leakages during the curing. The respective thicknesses of the TA6V4, the glue, and the composites were 0.4 mm, 0.150 mm, and 3.8 mm.

Two different mechanical strengths were obtained using different polymerizations of the epoxy glue, inducing different curing modes of the bonding. All the surfaces were first prepared by simple degreasing with ethanol. Lower (higher) mechanical strength was obtained by performing a

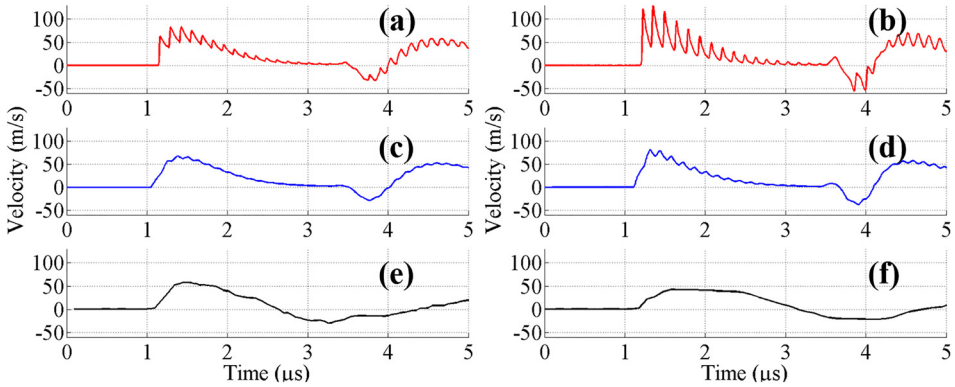

FIG. 2. FSV at the back face of the samples, when illuminating the TA6V4 (left) and the composite (right). Plots (a)–(d) are simulations with temporal resolutions of 0.1 ns (a) and (b) and 50 ns (c) and (d). Plots (e) and (f) are based on experiments (50 ns of temporal resolution).

polymerization of the glue of around 50% (90%) through modulating the curing of the bonding at 125 °C (150 °C) for 90 min (180 min) with ramps up and down (heating and cooling) of 2 °C/min. We used a laboratory oven to perform the curing, during which four spring clamps calibrated at 65 N maintained a constant strain. This process generates bonds with mechanical strengths of 15 and 35 MPa in the single-lap shear test for polymerizations at 50% and 90%, respectively, and pure longitudinal mechanical strengths of 10 MPa and 39 MPa, respectively. The last characterization was performed in accordance with the standard test method.[22] Even for the bonding of lower mechanical strength, its performances are close to many industrial bonding applications, for example, in ground transportation. The bond failure is adhesive for the partial (50%) reticulation, while it is cohesive for the reticulation at 90%.

The bonding dimensions allowed us to perform ten laser shots on a single sample with a distance of around 20 mm between each laser shot. This distance prevents failure propagation from one shot to another. The applied laser energy started at 10% of the energy available on the Hephaistos facility and was increased per 10% steps up to the maximum available. Water confinement was used. This procedure was applied to both bonding quality levels and when illuminating both surfaces of the structure. The back face was monitored using a photonic Doppler velocimetry (PDV) system to measure the free surface velocity (FSV) induced by the experiments. The time resolution of the PDV was 50 ns.

We first compare the simulations vs the experiments of the FSVs for an intensity of 3 GW/cm^2 for illuminations of TA6V4 and composite materials. The comparisons are presented in Fig. 2. On the left, we present the TA6V4 illumination, while the composite illumination is presented on the right. Plots (a) and (b) are the simulations directly obtained from ESTHER software, with a resolution time of 0.1 ns. Plots (c) and (d) are the simulations of (a) and (b) convolved with a low-pass filter, to obtain simulations of the same time resolution as the PDV [plots (e) and (f)]. For times shorter than 2.5 μs, a good correlation is observed between the convolved simulations (c) and (d) and the experimental detections (e) and (f), i.e., they are quite similar in shape and amplitude. For longer times, the simulated signal presents a decrease with an exponential shape after the arrival of the shock wave, while the shape of the experimental detection is more like a plateau. Moreover, the experimental negative velocities arrive earlier than the simulated ones, respectively, around 3 and 3.8 μs. Such differences are probably related to the real nature of the composite material vs the simulated one. Indeed, as ESTHER simulations are 1D, it can only model an isotropic material. Thus, the simulations performed here treat materials with properties intermediate between those of the composite fiber and the resin materials. In contrast, the experimental detection measures both contributions, leading to the observed decrease after the arrival of the shock wave with a plateau-like shape, as well as a starting time of the release wave earlier than the simulated one, with a longer duration.

Finally, we demonstrated the capability of the LASAT as an NDE of bonding quality. After the experiments, ultrasonic NDE of the samples was performed (under the same conditions as in the previous description) to identify the laser fluence debonding threshold. The results are presented in Table I. Highest (lowest) values of the uncertainties correspond to the first (last) laser fluence where (before) debonding appears. The threshold is defined as the midpoint between the uncertainty values. The corresponding tensile stresses simulated using ESTHER are also presented. First, the two bonding qualities are clearly discriminated: the debonding of the lowest mechanical strength appears for intensities around 2.7 ± 1 GW/cm^2, while the highest bonding debonds at intensities around 4.7 ± 1 GW/cm^2. These differences are in good agreement with the quantifications of the longitudinal and transverse mechanical strength of the different bonds. Second, for both bonds, the failure appears at ~25% lowest energies when illuminating the composites compared to when illuminating TA6V4. These results are in

TABLE I. Experimental laser fluencies and corresponding simulated tensile values to induce bonding failure for the TA6V4 and 3D-CFRP illuminations. Error bars are defined by experimental laser fluence steps.

Mechanical strength	Good		Bad	
Illuminated surface	T Λ6V4	3D-CFRP	T Λ6V4	3D-CFRP
Laser fluency (GW/cm^2)	5.2 ± 0.54	4.2 ± 0.49	3.2 ± 0.49	2.25 ± 0.39
Simulated tensile value (MPa)	310 ± 20	300 ± 20	260 ± 20	250 ± 20

good agreement with the previous discussion, as illumination of the composite instead of TA6V4 increases the tensile strain by ∼20% at the epoxy interfaces. Thus, using the ESTHER simulations, we finally identified the required tensile stress to induce debonding at the epoxy interfaces, being 310 MPa for the highest mechanical strength and 260 MPa for the lower.

To conclude, we have studied the acoustic phenomena involved in the LASAT process of a TA6V4/composite bond. Such phenomena are more complex than expected and are related to the break of acoustic impedance in the studied bonding. Moreover, we have presented the first nondestructive quantification of the mechanical strength of a structural bond. These results were obtained for aeronautical materials bonded with an aeronautical-quality bond. Thus, it paves the way for a routine method of structural bonding certification, which could help the aviation industry to achieve its collective targets for CO_2 emission reduction. For the maturation of the technology, the next steps should be 3D simulations, taking into account the complex reflection/transmission laws of shock waves,[23] and an optimization of the experimental illumination of the structure, with two laser pulses onto each face of the structure.[24]

We gratefully acknowledge the support of BPI France, Ile de France, Nouvelle Aquitaine regions, and competitiveness clusters ASTECH, Route des Laser and Aerospace Valley through the CompoChoc project for this work.

[1]Global Aviation Industry, www.atag.org for the working paper developed for the 38th ICAO Assembly September/October 2013, available at https://www.realwire.com/writeitfiles/PositionPaper_ICAO-ASBY_2013_mediumres.pdf.

[2]Federal Aviation Administration, *Advisory Circular-Composite Aircraft Structure* (Federal Aviation Administration, 2009).

[3]K. B. Katnam, L. F. M. Da Silva, and T. M. Young, Prog. Aerosp. Sci. **61**, 26 (2013).

[4]M. Grossmann, M. Schubert, C. He, D. Brick, E. Scheer, M. Hettich, V. Gusev, and T. Dekorsy, New J. Phys. **19**, 053019 (2017).

[5]E. Siryabe, M. Rénier, A. Meziane, J. Galy, and M. Castaings, Ultrasonics **79**, 34 (2017).

[6]E. Siryabe, M. Rénier, A. Meziane, and M. Castaings, Phys. Proc. **70**, 541 (2015).

[7]S. Mezil, J. Laurent, D. Royer, and C. Prada, Appl. Phys. Lett. **105**, 021605 (2014).

[8]B.-Y. Chen, S.-K. Soh, H.-P. Lee, T.-E. Tay, and V. Tan, J. Compos. Mater. **50**, 3089 (2016).

[9]L. Berthe, M. Arrigoni, M. Boustie, J. P. Cuq-Lelandais, C. Broussillou, G. Fabre, M. Jeandin, V. Guipont, and M. Nivard, NDT & E Int. **26**, 303 (2011).

[10]L. Berthe, R. Fabbro, P. Peyre, L. Tollier, and E. Bartnicki, J. Appl. Phys. **82**, 2826 (1997).

[11]M. Perton, A. Blouin, and J.-P. Monchalin, J. Phys. D **44**, 034012 (2011).

[12]B. Ehrhart, R. Ecault, F. Touchard, M. Boustie, L. Berthe, C. Bockenheimer, and B. Valeske, Int. J. Adhes. Adhes. **52**, 57 (2014).

[13]M. Ansar, W. Xinwei, and Z. Chouwei, Compos. Struct. **93**, 1947 (2011).

[14]ASTM, *Standard Test Method for Compressive Residual Strength Properties of Damaged Polymer Matrix Composite Plates*, *ASTM D7137/D7137M-12* (ASTM, 2012).

[15]S. Bardy, B. Aubert, L. Berthe, P. Combis, D. Hébert, E. Lescoute, J.-L. Rullier, and L. Videau, Opt. Eng. **56**, 011014 (2016).

[16]M. Born and E. Wolf, *Principles of Optics*, 7th ed. (Cambridge University Press, 2006).

[17]J.-P. Colombier, P. Combis, R. Stoian, and E. Audouard, Phys. Rev. B **75**, 104105 (2007).

[18]R. Ramis, K. Eidmann, J. Meyer-ter-Vehn, and S. Hüller, Comput. Phys. Commun. **183**, 637 (2012).

[19]D. R. Jones, D. J. Chapman, and D. E. Eakins, J. Appl. Phys. **114**, 173508 (2013).

[20]D. Laporte, Ph.D. Manuscript, ENSMA, France, 2011.

[21]M. Hamilton and D. Blackstock, *Nonlinear Acoustics* (Academic Press, San Diego, 1998).

[22]ASTM, *Standard Test Method for Pull-Off Strength of Coatings Using Portable Adhesion Testers*, *ASTM D4541-17* (ASTM, 2017).

[23]R. Marchiano, S. Baskar, F. Coulouvrat, and J.-L. Thomas, Phys. Rev. E **76**, 056602 (2007).

[24]M. Ghrib, L. Berthe, N. Mechbal, M. Rébillat, M. Guskov, R. Ecault, and N. Bedreddine, Compos. Struct. **171**, 286 (2017).